Disponible en www.hormigonyacero.com
Hormigón y Acero, 2026
https://doi.org/10.33586/hya.2026.4208

ARTÍCULO EN AVANCE ON LINE

Experimental Measurement of the Response of a Linear Elastic Structure to Blast Loading. Validation of Load Models and Simplified Analysis Methodologies

M. Chiquito, A. Pérez-Caldentey, A.P. Santos, R. Castedo, L.M. López, D. Cendón, F. Gálvez

DOI: https://doi.org/10.33586/hya.2026.4208

Para ser publicado en: *Hormigón y Acero*

Por favor, el presente artículo debe ser citado así:
Chiquito, M., Pérez-Caldentey, A., Santos, A.P., Castedo, R., López, L.M., Cendón, D., & Gálvez, F. (2026) Experimental Measurement of the Response of a Linear Elastic Structure to Blast Loading. Validation of Load Models and Simplified Analysis Methodologies, *Hormigón y acero,* https://doi.org/10.33586/hya.2026.4208

Experimental Measurement of the Response of a Linear Elastic Structure to Blast Loading. Validation of Load Models and Simplified Analysis Methodologies.

M. Chiquito[a,*], A. Pérez-Caldentey[b,c], A.P. Santos[a], R. Castedo[a], L.M. López[a], D. Cendón[b], F. Gálvez[b]

[a] *E.T.S.I. de Minas y Energía. Universidad Politécnica de Madrid. España.*

[b] *E.T.S.I. de Caminos, Canales y Puertos. Universidad Politécnica de Madrid.*

[c] *FHECOR Consulting Engineers*

[*] Corresponding author:

e-mail: maria.chiquito@upm.es

Tlf. (+34) 91 067 65 28

ABSTRACT

This paper focuses on part of the experimental program of research project ITSAFE. ITSAFE is a project, aimed at developing a response methodology to a bomb threat occurring inside an important transport infrastructure. Such a methodology was felt to be an urgent need by security officials who were interviewed during a previous project, as a basis for fast decision-making when facing a given threat.

The first part of the project, which is the focus of this paper, consisted in evaluating by measurement the effect of the action. This has been done by designing a steel structure able to resist three different levels of blast load exhibiting a linear elastic response. In this way it is possible, not only to directly measure the pressure wave attaining the structure, but also to assess whether or not the response of the structure is consistent between the measured time-pressure curves, theoretical dynamic calculations and finite element numerical models using LS-DYNA. This evaluation is greatly simplified and made more accurate by the fact that the response is linear elastic. Results show that it is possible to

approximate the problem with some confidence, both by numerical and analytical methods.

Keywords: Blast loading; pressure measurements; structural response; high frequency dynamic measurements

1 Introduction

In the last decades, the necessity to understand the response mechanism to blast loading of different types of structures and the need for new protective solutions has become more pressing. This is due to the increased risk that structures may be subjected to blast loads due to accidental events or intentional terrorist attacks. For instance, the Global Terrorism Index 2026 indicates a 280% increase in terrorism-related deaths in 2025 [1]. Methods for analysis of the structural responses to blast loads can be categorized into three main approaches: simplified analytical methods, numerical simulations, and experimental tests [1,2].

Analytical methods are commonly used to predict the global response of a structure subjected to blast loading. These methods include the idealization of the structure by using a single degree of freedom (SDOF) or multi degree of freedom (MDOF) systems. Biggs [2] has systematically studied the maximum displacement response spectra of the SDOF system under triangular loading, which is a simplification that can be used to model bast loading. These results have been widely adopted for global damage assessment of the structural response to blast loading in the early design [3–5]. However, this analytical method is unable to account for secondary modes of vibrations. Therefore, numerical methods such as finite element method (FEM) appear as a good alternative to predict the structural response under blast loads more accurately. There are many different available

codes capable of reproducing both, the blast wave pressure as well as the structural behaviour. All of them can provide good results when compared to experimental tests. For this reason, many authors have studied blast effects on structures by means of numerical modelling [6–9]. However, blast is a highly dynamic phenomenon with a very short duration and very fast propagation of strain waves which complicates the analysis and understanding of the problem. Moreover, the variations in scenarios and structural typologies, etc. are very large, making it necessary to validate the numerical results by means of experimental tests.

There have been many experimental programs aimed at the evaluation of the resistance of structures to blast loads [10,11] . However, in many cases, these experimental programs are intended to damage the tested structure, and it is not easy to obtain detailed information regarding the applied load from the measurement of the structural response. Most of the experiments are designed to test different types of retrofitted elements by comparing them with non-reinforced elements [12–14]. On the contrary, the tests presented in this paper were aimed at evaluating the action by measuring the response of a simple structure.

This paper focuses on part of the experimental program of research project ITSAFE. ITSAFE is a project, sponsored by the Spanish Ministry for Economy and Competitivity. It is aimed at developing a response methodology to a bomb threat occurring inside an important transport infrastructure, such as an airport terminal. For such cases, the magnitude of the explosive loads is assumed to be limited to that which can be transported in a backpack, which can easily be introduced inside an infrastructure. Such a methodology was felt to be an urgent need by security officials who were interviewed during a previous project, as a basis for fast decision-making when facing a given threat. In the following sections, the process of designing the specimen, and the test results will

be detailed. Design was carried out using very simple procedures based on a single degree of freedom system. For this purpose, a steel structure was designed to withstand three different levels of blast load exhibiting an elastic response. In this way it was possible not only to directly measure the pressure wave attaining the structure, but also to assess whether the response of the structure is consistent with the measured pressure-time curves. The uncertainties in modelling and the number of parameters involved were greatly reduced by the fact that the response is linear elastic and the material behaviour well known.

The paper discusses the design of the specimen, summarizes the results of the tests, and compares the predictions of a finite element model with the experimental values.

2 Design of the test specimens and preliminary behaviour predictions

It was decided that a simply supported element with a relatively significant area would be the easiest to analyse. The explosive load could be placed over the element and measuring devices could be placed under the element which would act as a protective shield for the sensors. After some preliminary analyses, the geometry shown in Figure 1 was adopted. The structure consisted of three HEB-360 steel profiles of 4.00 m span, on which a 40 mm thick steel plate of 4500 mm length and 2388 mm width was welded. In addition, the profiles were joined by a transversal diaphragm formed by vertical and horizontal 10 mm stiffener plates welded to the profiles in the area of the supports to ensure proper load transfer. The material used for the construction was S275 steel for the steel beams and stiffeners and S355 steel for the top plate.

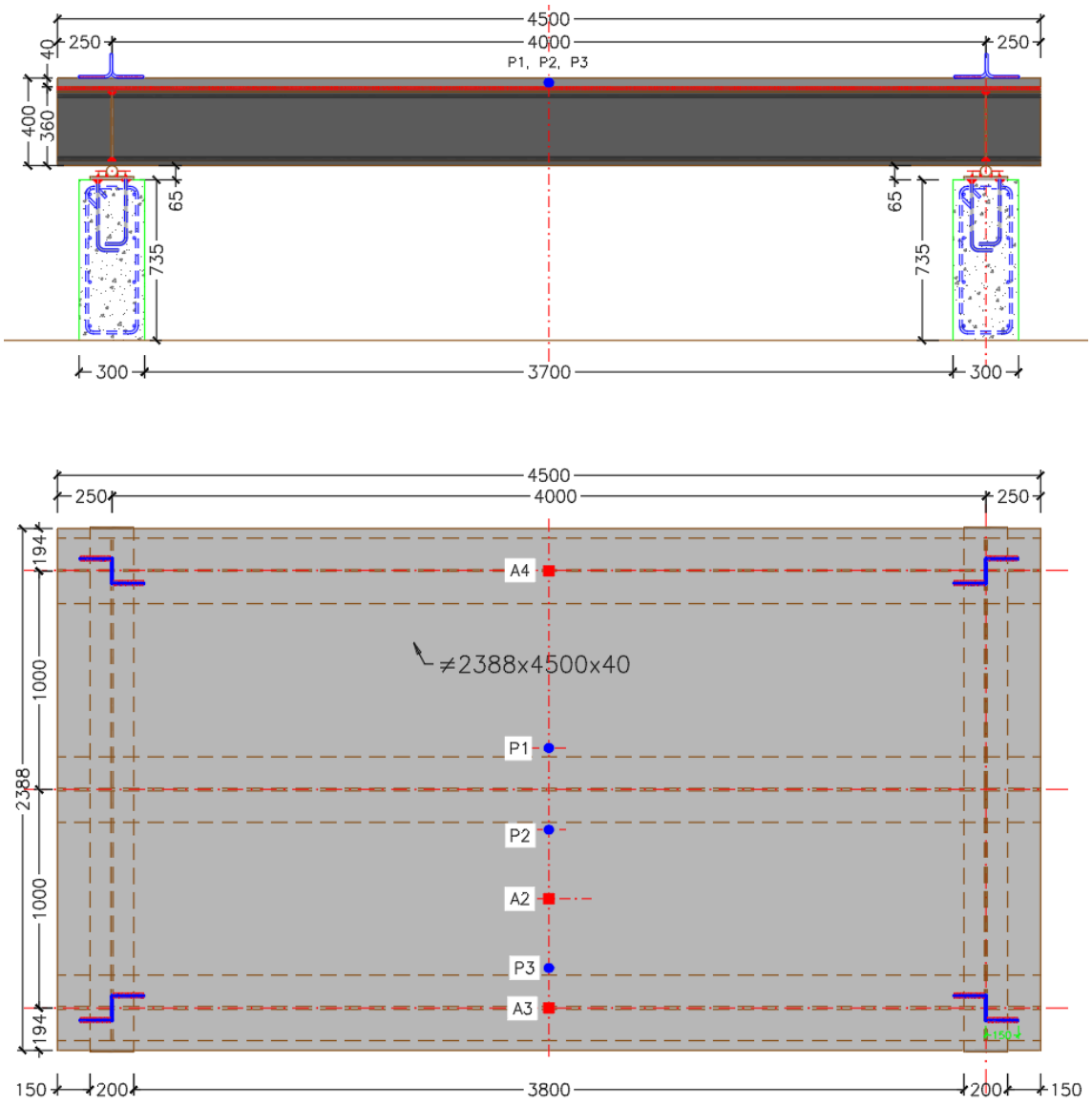

Figure 1 Test specimen. a) plan view; b) front view (units: mm).

The specimen was subjected to four different explosion tests. For this purpose, three spherical shaped blast loads of 0.8 kg, 2.0 kg (two tests) and 3.2 kg of TNT equivalent were used. In all cases, the charge mass was placed hanging from a rope at a distance of 2.5 m from the centre of the top face of the steel plate of the specimen. Figure 2 shows the set-up of the specimen before testing.

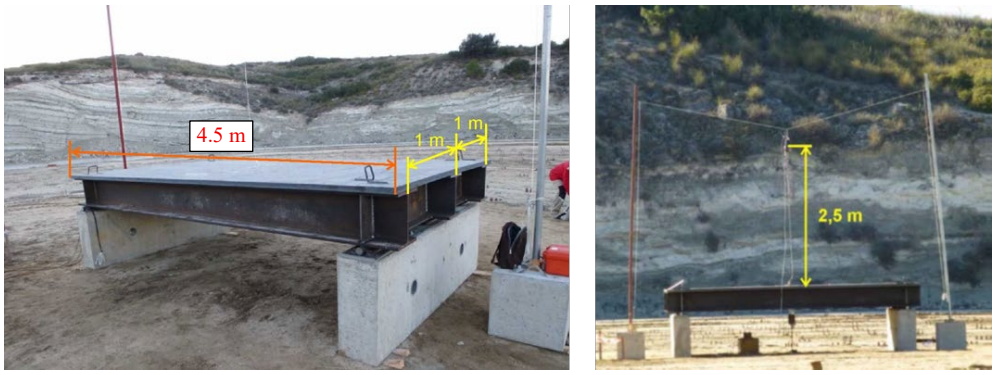

Figure 2 View of the specimen before testing.

The monitorization used is represented in Figure 3 and Figure 4 (see also Figure 1) which shows the position of three piezoelectric pressure gauges (mounted on the upper face of on the top plate) with a sampling rate of 500 kHz and a sensitivity of 10 mV/PSI (P1, P2 and P3), as well as four accelerometers with a range of 5000 g, a resolution 0.02 g and a resonance frequency greater than 100 kHz) (A1 through A4). Additionally, the deflection was measured by means of a high frequency laser (MEL M70LL with a measuring frequency of 100kHz). This measurement is very important as it is not an easy task to obtain reliable values of deflections by double integration of accelerations since it involves correcting drift and filtering frequencies. Having an independent reference of direct measurement of deflections is therefore a very valuable aid. Additionally, the test was filmed using a high-speed camera with a frame speed of 8000 frames per second.

The response of the structure was evaluated in a simplified manner using a single degree of freedom system. This methodology was used for the design of the specimens and the expected behaviour was then evaluated using a LS-DYNA model, in order to have a more precise evaluation.

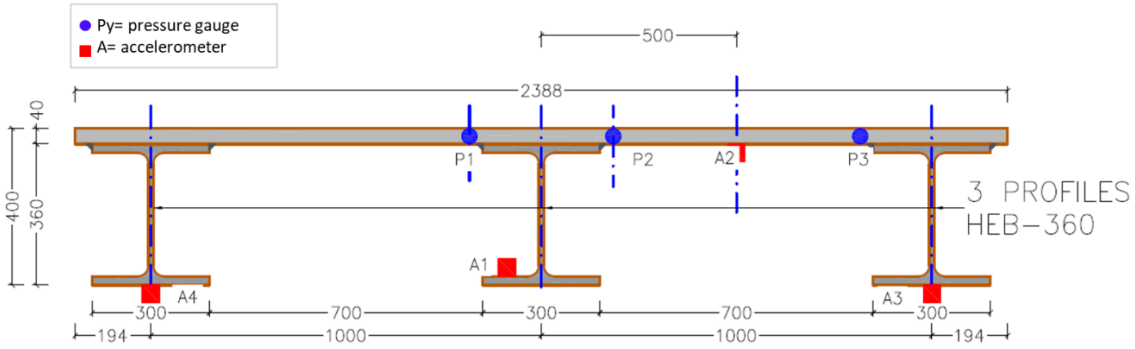

Figure 3 Mid-span transversal section: Details of monitoring used.

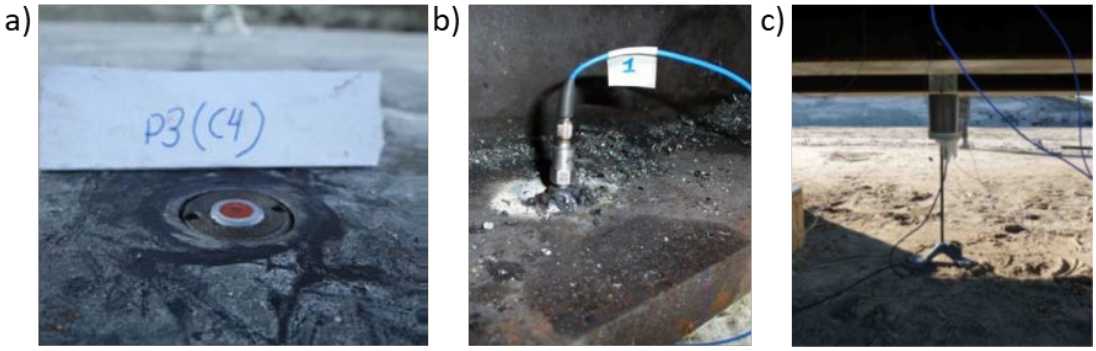

Figure 4 Measuring devices used in the test: a) pressure transducer; b) accelerometer; c) high frequency laser.

In summary, the simplified analysis methodology described in [15] is carried out in the following four steps:

1. Determine an equivalent single degree of freedom (SDOF) system representative of the structure (See Figure 5). This can be done following, for instance, the methodology of Biggs, 1964 [2]. Given an assumed shape function $\phi(x)$, describing the displacements of the structure, $\delta(x)$, divided by the displacement at the point of maximum deflection, δ_{max}, ($\phi(x) = \delta(x)/\delta_{max}$), the equivalent mass M_E, the equivalent applied load P_E, and the equivalent stiffness K_E, of the SDOF are given – from considerations of equivalence of energy between systems – by the expressions of Eq. (1). These expressions are applied to the case of a beam of constant distributed mass, m, along the x-axis of the element and

subjected to a constant distributed load, q, to which the steel structure will be assimilated. The values of K_M and K_L are provided in many textbooks for different support conditions and load patterns. In the case of the structure being tested, assuming it can be assimilated to a simply supported beam, the values for these coefficients are $K_L=2/\pi\sim0.64$ and $K_M=0.50$. Also, for a simply supported beam, constant $k=5/384$. The first natural period, T_E, of the SDOF system is determined using Eq. (2).

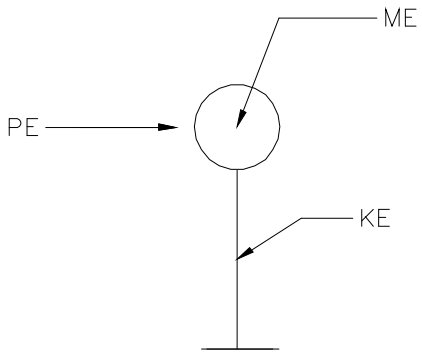

Figure 5 Single degree of freedom system.

$$\begin{aligned} M_E &= \int_0^L m(x)\phi^2(x)dx \rightarrow M_E = K_M mL \\ P_E &= \int_0^L q(x)\phi(x)dx \rightarrow P_E = K_L qL \\ K_E &= \frac{P_E}{\delta_{max}} = \frac{K_L qL}{k\frac{qL^4}{EI}} = \frac{K_L}{k}\frac{EI}{L^3} \end{aligned} \tag{1}$$

$$T_E = 2\pi\sqrt{\frac{M_E}{K_E}} \tag{2}$$

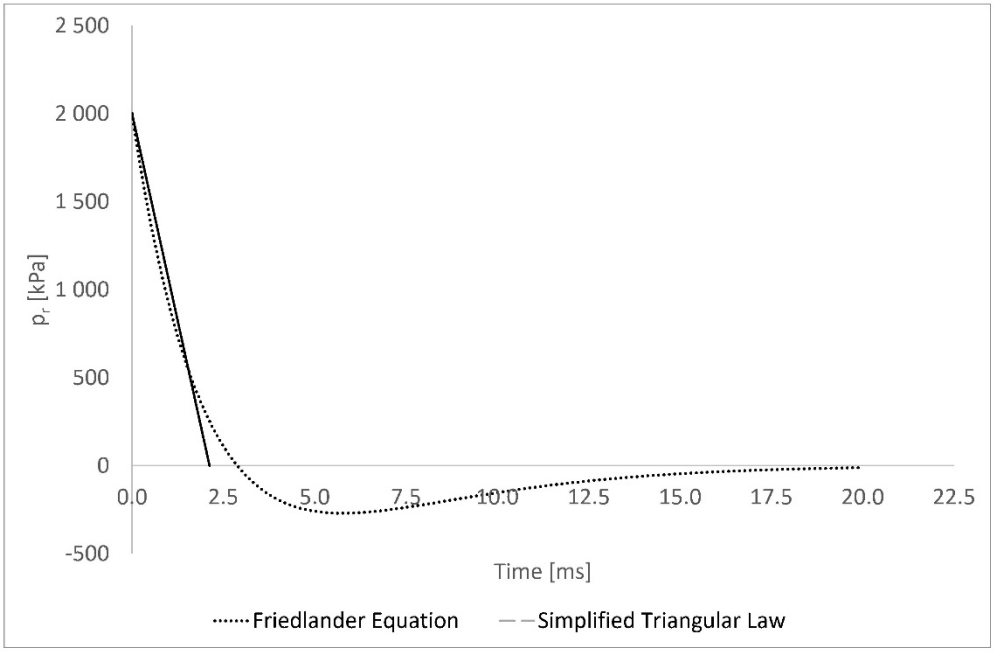

Figure 6 Friedlander curve and simplified triangular law.

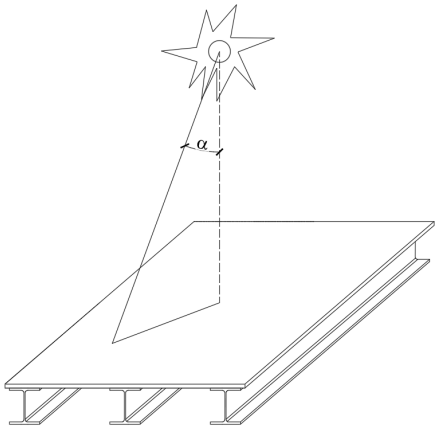

Figure 7 Definition of angle of incidence, α.

2. Determine the load acting on this system. For this, the blast load is assimilated to a triangular pressure-time load which has the same impulse as the positive phase of the pressure-time curve (see Figure 6). The negative phase of the pressure-time curve is neglected. This load is determined from the UFC 3-340-02 Manual [16]. The maximum reflected pressure $P_{r,\alpha}$ [kPa] is determined for a given angle of incidence of the pressure front with respect to the surface of the structure. Then, the scaled impulse, $i_{r,\alpha}$ (i.e. the impulse divided by the cubic root of mass of the

explosive) is also determined depending on the angle of incidence (see Figure 7), which for the simplified analysis is taken as 90º(the FEM analysis, however, accounts for the varying distance and the incidence angle, using the formulation of [16], which is implement as a standard feature in LS-DYNA). Finally, the duration of the triangular pressure-time curve is determined from the scaled impulse, $i_{r,\alpha}$ by applying Eq. (3).

$$t_{rf} = \frac{2i_{r,\alpha}}{P_{r,\alpha}} \sqrt[3]{m} \tag{3}$$

3. Using the expressions for the behaviour of a SDOF system subjected to triangular loading, the Dynamic Load Factor (DLF), that is, the ratio of the dynamic to static deflection, can be determined. A solution for this problem is given in Biggs, 1964 [2] and reproduced herein (see Eq. (4)).

$$\begin{aligned} \omega &= \frac{2\pi}{T_E} \\ DLF &= 1 - cos\,\omega\, t + \frac{sin\omega t}{\omega \cdot t_{rf}} - \frac{t}{t_{rf}} \quad \text{if} \quad t \le t_{rf} \\ DLF &= \frac{1}{\omega t_{rf}}\left[sin\omega t - sin\omega\left(t - t_{rf}\right)\right] \\ &\qquad - cos\,\omega\, t \quad \text{if} \quad t > t_{rf} \end{aligned} \tag{4}$$

4. Determine the deflections and forces from a static analysis using a load equal to $P_{r,\alpha} \times DLF$.

For illustrative purposes, this analysis is detailed for the 2.0 kg TNT equivalent load. The central beam is considered as a simply supported structure. The equivalent SDOF system is determined assuming the behaviour of the structure can be assimilated to that of the central beam with the section shown in Figure 8. The width of 909 mm corresponds to the effective width according to EN 1993-1-5:2006 [17].

$$b_{eff} = 2b_0 \frac{1}{1 + 6.4\frac{b_0}{L}} = 2 \times 0.5 \frac{1}{1 + 6.4\left(\frac{0.5}{4}\right)^2} = 0.909\ m \tag{5}$$

In Eq. (5), b_0 is half the distance between beams and L is the distance between points of zero bending. b_{eff} is used to determine the inertia of the section (I_y). The area A (which will be used to determine the mass), includes the full width assigned to the central profile.

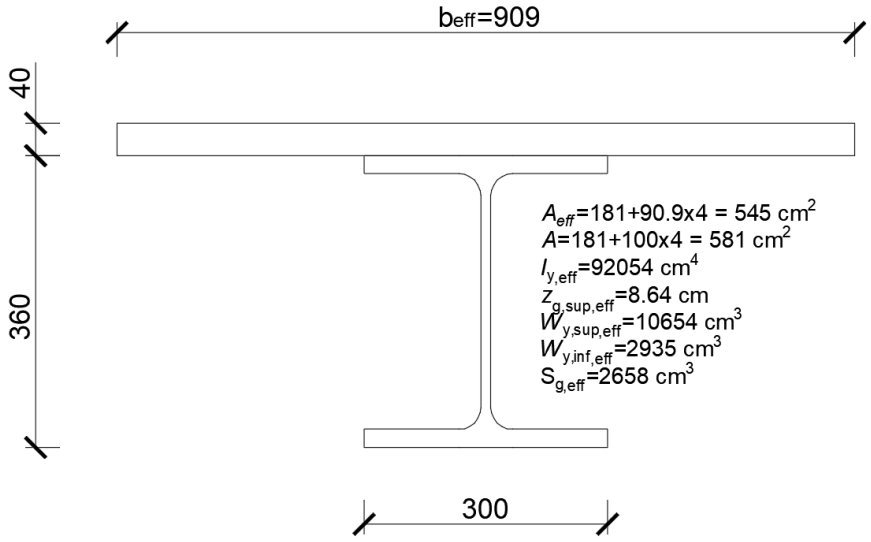

Figure 8 Cross section and geometrical properties of the central beam.

From Eqs. (1) and (2) and the cross-section properties of Figure 8, the fundamental eigen-period of the system can be calculated:

$$M_E = K_M mL = 0.5 \times 0.0581 \times 7.85 \times 4 = 0.912 \text{ t}$$
$$K_E = \frac{K_L}{k}\frac{EI}{L^3} = \frac{0.64}{\frac{5}{384}}\frac{2 \times 92054}{4^3} = 141395\ kN/m \quad (6)$$
$$T_E = 2\pi\sqrt{\frac{M_E}{K_E}} = 2\pi\sqrt{\frac{0.912}{141395}} = 0.016\ s$$

The first natural period is therefore close to 16 ms, which corresponds to a frequency of 62.5 Hz.

Table 1 contains the data necessary to obtain the displacements for each test according to the equivalent SDOF system: mass of explosive (TNT equivalent), m, distance of charge to the top plate surface, d, scaled distance, Z, reflected pressure, P_r, duration of the equivalent triangular load, t_{rf}, reflected impulse, i, dynamic load factor, DLF, equivalent load to be applied to the SDOF system, P_E, and maximum deflection obtained by dividing

the equivalent load by the equivalent stiffness (K_E=141395 kN/m). Table 2 contains the maximum resulting forces applied on the structure (bending moment, M_{max}, and shear force, V_{max}) as well as the normal stresses at the top and bottom of the section (σ_{sup} and σ_{inf}) and the maximum shear stress (at the neutral axis), τ_{max}. To determine the maximum moment and shear, the equivalent distributed load is determined from the expression shown in the following equation:

$$q = P_r \times DLF \times 2b_0$$

$$M_{max} = \frac{qL^2}{8} \quad V_{max} = \frac{qL}{2} \tag{7}$$

Such an analysis can be carried out quite easily, as can be seen, and should always be the first approximation used to validate more complex procedures. From the stresses obtained in this table it is clear that the behaviour of the structure remains within the elastic range.

Table 1 Summary of expected results from simplified analysis: deflections.

Test #	m [kg]	d [m]	Z [m/kg$^{1/3}$]	P_r [kPa] [16]	t_{rf} [ms] [16]	i [kN.ms] Eq. (3)	DLF Eq. (4)	$P_r \times DLF$ [kPa]	P_E [kN] Eq. (1)	δ [mm]
1	0.8	2.5	2.693	265	1.15	152.3	0.224	59	152	1.07
2/3	2	2.5	1.984	643	0.94	345.1	0.183	118	301	2.13
4	3.2	2.5	1.697	1137	0.77	439.1	0.151	172	443	3.11

*Table 2 Summary of expected results from simplified analysis: forces and stress*es.

Test #	M_{max} [kNm]	V_{max} [kN]	σ_{sup} [MPa]	σ_{inf} [MPa]	τ_{max} [MPa]
1	118.74	118.74	-11.15	40.45	26.64
2/3	235.34	235.34	-22.11	80.16	52.80
4	343.37	343.37	-32.25	116.96	77.04

3 Test results

Four tests referred to as E1 to E4 were finally carried out. This is because test number two (E2), with a blast load of 2.0 kg of TNT equivalent mass, was repeated due to a malfunction of some of the sensors.

Figure 9 shows a sequence of images taken by a high-speed camera producing 8000 images per second. These images allowed to visualize the pressure front and measure the arrival time of the shock wave to the structure's surface.

Figure 9 Sequence of images of test number 4 (3.2 kg TNT equivalent) taken with the high-speed camera.

Regarding the results measured using pressure sensors and accelerometers, two of the acceleration-time and pressure-time curves registered are given, as examples, in Figure 10. These correspond to Test E1 (0.8 kg of TNT equivalent mass).

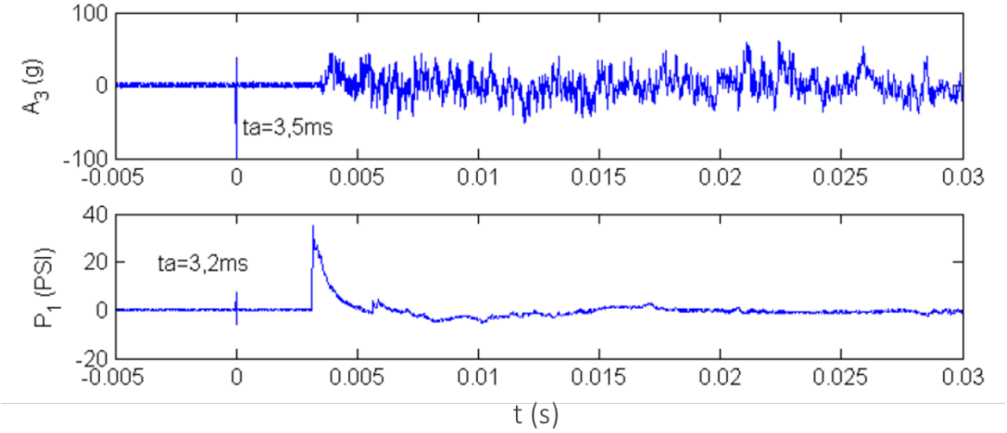

Figure 10 Example of acceleration-time and pressure-time histories (test E-1).

3.1 Pressure results

A more comprehensive view of pressure results is provided in Table 3. The table provides the mass of the explosive in TNT equivalent, *W_TNT*, the distance from the explosive to the top of the structure, *d*, the scaled distance, *Z*, the measured peak reflected pressure corresponding to the positive phase, $P_{r,exp}+$, the impulse of the positive phase, $I_{r,exp}+$, the duration of the positive phase, $t_{0,exp}+$ (note that this value is different from the t_{rf} value for the equivalent triangular pressure diagram used above for the SDOF equivalent model) and the arrival time t_a. Some of the sensors did not record proper signals during the test and hence are not listed in Table 3. Furthermore, the pressure and impulse data from the P1 and P3 sensors in tests E3 and E4 were considered less reliable due to a problem detected in the signal feed. However, this problem did not affect the arrival times (t_a).

A comparison between these values and the values provided by the UFC 3-340-02 Manual [16] is provided in Figure 11. It can be seen that good agreement is obtained between measured and UFC 3-340-02 values. The measured values also match the orders of

magnitude estimated in Table 1, especially in terms of the reflected impulse which is the most significant parameter.

Table 3 Results from pressure sensors.

Tests	E1		E2	E3			E4		
Sensor	P1	P3	P2	P1	P2	P3	P1	P2	P3
W_TNT (kg)	0.8	0.8	2.0	2.0	2.0	2.0	3.2	3.2	3.2
d (m)	2.5	2.6	2.5	2.5	2.5	2.6	2.5	2.5	2.6
Z (m/kg$^{1/3}$)	2.7	2.8	2.0	2.0	2.0	2.1	1.7	1.7	1.8
$P_{r,exp}$+ (kPa)	240.8	179.4	673.0	-	841.3	-	-	1393.0	-
$I_{r,exp}$+ (kPa.ms)	134.8	111.8	299.1	-	329.6	-	-	436.0	-
$t_{0,exp}$+ (ms)	2.1	1.9	1.7	1.7	1.7	1.9	1.5	1.4	2.0
t_a (ms)	3.2	3.5	-	2.3	-	2.6	2.0	-	2.2

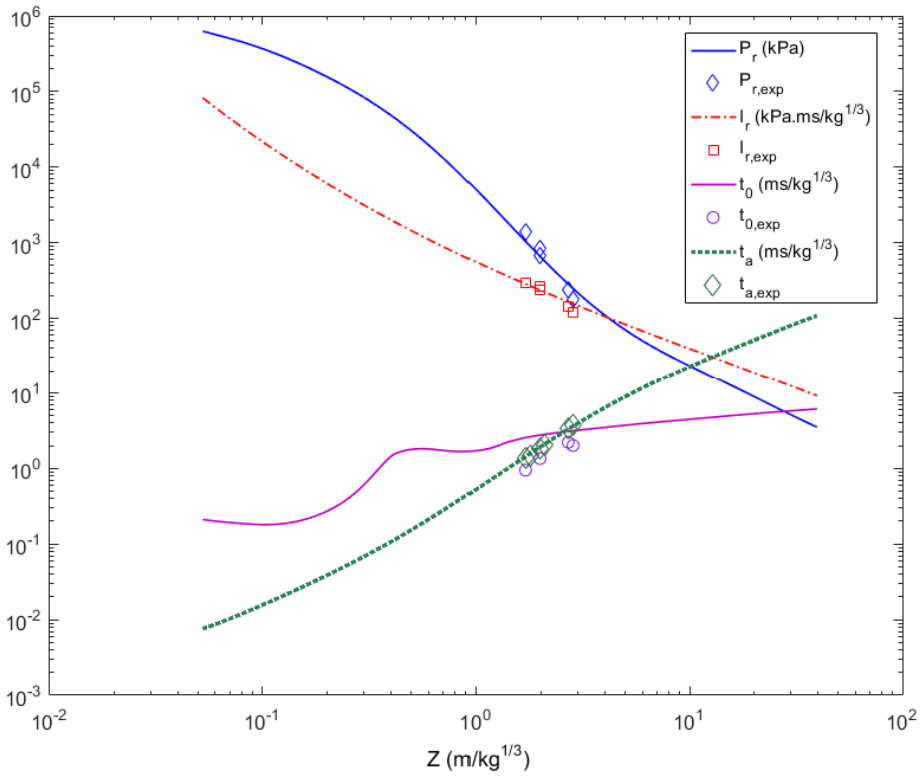

Figure 11 Comparison between measured values and the curves provided by UFC 3-340-02[16].

3.2 Acceleration results

In all tests, four measurements were obtained, except in test E2 where only sensors A2 and A4 produced recordings. In the recordings obtained in test E1, where the explosive

mass was the lowest, no drift or direct current (DC) offset was visible. In tests E2 and E3, with an intermediate explosive load, the quality of the signals decreased and the signals with sensor A2 reached saturation at certain times; sensors A1 and A3 did not record any events in test E2. In test A4, with the highest load, the signals from sensors A2 and A4 had a strong drift that caused saturation for most of the recording. These signals were discarded for further analysis, together with the acceleration obtained with A3 which, except in the first instants (times less than 8 ms), measured a constant acceleration of about 250g.

Table 4 shows the peak values, positive and negative, of acceleration obtained in the first stages of the test (times less than 20 ms). Contrary to what might be expected, in three signals (records with A2 and A4 in test E2 and signal with A1 in test E3) the highest acceleration in absolute value is obtained when the structure moves upwards, while in the rest of the records the acceleration peak is obtained when the panel moves downwards.

Table 4 Acceleration results.

Test	Sensor	Acceleration (*g*)	
		Negative (upwards)	Positive (downwards)
E1	A1	-90.4	124.6
	A2	-125.3	155.3
	A3	-52.1	60.8
	A4	108.1	114.7
E2	A2	-502.5	486.4
	A4	-405.7	351.2
E3	A1	-384.4	173.8
	A2	-433.7	473
	A3	-379.8	443.3
	A4	-428.9	451.9
E4	A1	-245.7	424.9

3.3 Displacement results

The displacement-time histories obtained with the high frequency laser in the four tests are shown in Figure 12. In test E1, the time baseline was different from the rest of the

tests and the displacement had an offset of -2 mm (Figure 12, upper graph). In the first moments of the recordings obtained in tests E2, E3 and E4 (lower graph), atypically high displacements were obtained, probably due to the fireball blinding the laser signal. After about 3 ms, this effect disappeared, and the laser measured the displacement experienced by the panel; this instant is marked with a circle in Figure 12. In test E1 (Figure 12, upper graph), in which the time origin was unknown and cannot be related to any event in the test, it seems that the start of the panel movement occurred after about 10 ms; note that from this instant onwards the recording has a similar shape to that of tests E2, E3 and E4 (lower graph). There was also an offset in the displacements obtained in tests E3 and E4 with respect to those measured in E1 and E2, so that the displacement in tests E2 and E3, in which 2 kg were used, is different.

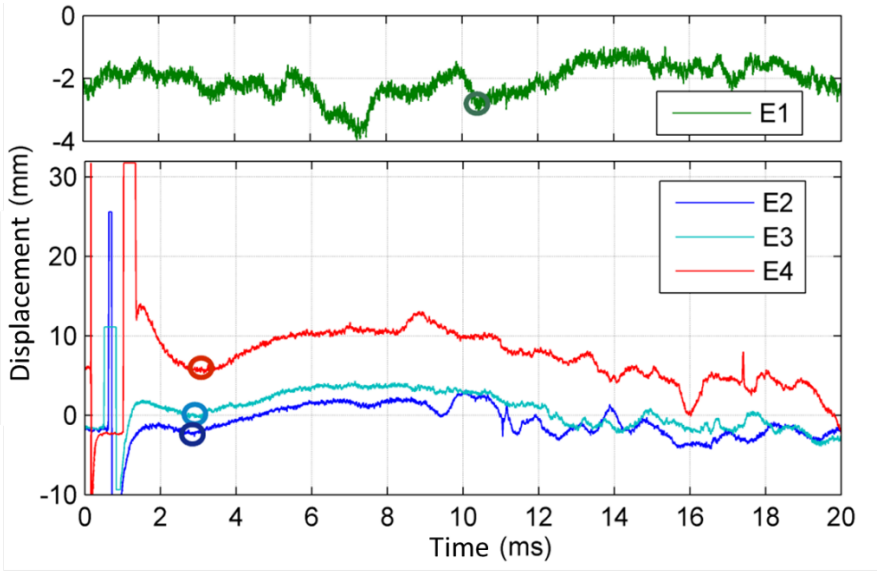

Figure 12 Raw displacement signals; E1 test in the upper graph and E2 to E4 tests in the lower graph.

Figure 13 shows the processed displacement signals. The noise presented in the displacement measurements has been smoothed using a weighted local regression with a band window of 5 % of the signal length. The signals have been normalised with respect to the displacement and time of the points marked in Figure 12.

The half-period of the processed displacement varies between 9.5 ms (tests E1, E2 and E3) and 10.6 ms (test E4), which corresponds to a frequency of about 50 Hz. This value is close to the frequency calculated above for the first vibration mode of the whole structure. The maximum displacement values have been obtained from the maximum of the quadratic function fitted to the positive part of the record; these values are shown in Table 5. Table 5 shows two values, the absolute maximums and the maximums obtained by ignoring local variations in registries of E2 and E4, which are attributed to signal noise, since the plate should deform following a fairly smooth sine curve with the estimated period. These values are given as "softened in the table." These softened values agree reasonably well with the values estimated in Table 1 (as shown numerically in Table 6, below).

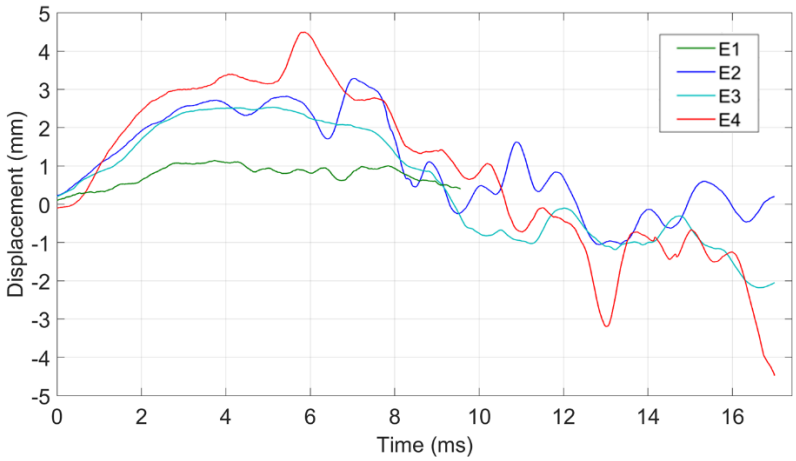

Figure 13 Processed displacement signals.

Table 5 Result of maximum displacement.

	Test			
	E1	E2	E3	E4
Displacement (mm)	1.05	3.29	2.53	4.50
Softened displacement (mm)	0.95	2.70	2.53	3.20

4 Numerical model

In addition to the simplified predictions obtained with SDOF system, a finite element (FE) model was developed using the LS-DYNA code. The objective was to assess whether or not the response of the structure is consistent between the measured displacement-time histories, theoretical dynamic calculations, and finite element numerical models.

The model geometry is shown in Figure 14. The steel plate and the three steel profiles were modelled as well as the support diaphragms, formed by the horizontal and vertical stiffeners welded to the longitudinal beams and to the top plate. The numerical model was built using shell elements. This type of element helps to reduce the computational time, without losing precision in the calculation.

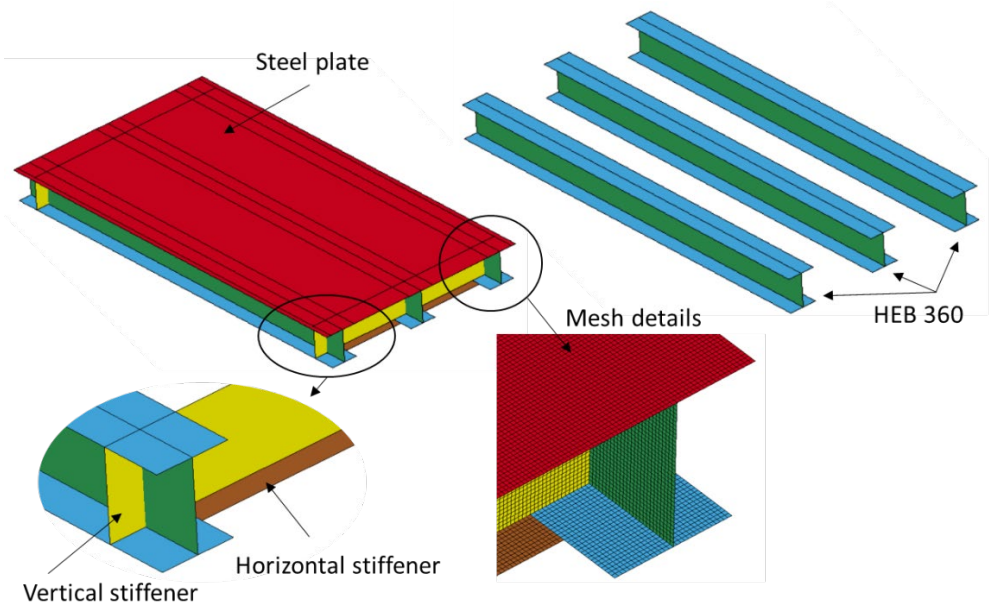

Figure 14 Details of the geometrical model.

Regarding the mesh size, a mesh sensitivity test was conducted, as the accuracy of the numerical result is dependent on the mesh size. A constant ratio for the mesh refinement was used starting with 20 mm, then 10 mm and finally 5 mm. The same mesh size was used for all elements as shown in Figure 14. The study was conducted for tests E2/E3

where the explosive mass detonated was 2kg of TNT equivalent. After checking the maximum displacement results, a difference of 0.001 mm (an error smaller than 0.05%) could be observed between the two smallest mesh sizes (see Figure 15), so 10 mm was finally used in the numerical models.

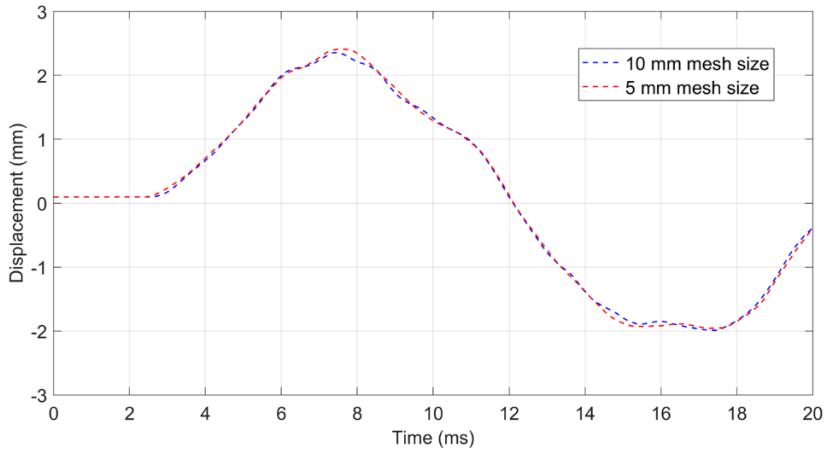

Figure 15 Result of displacement obtained in test E2/E3 for the mesh sensitivity test.

Since the structure was built using steel, an elasto-plastic material was used in the numerical simulation. However, the plastic branch is not expected to play a role here. This material model is defined in LS-DYNA using the piecewise linear plasticity material type 24. The mechanical properties needed to define the material model were the material density (7850 kg/m^3), Young's modulus (210 GPa), Poisson's ratio (0.3) and the yield strength (275 MPa for beams and stiffeners and 355 MPa for the top plate).

As for the blast loading, the load blast enhanced (LBE) technique was used. This feature defines an air blast function for the application of pressure loads based on equations derived by Kingery and Bulmash [18]. With this technique, only the coordinates of the charge centre, the TNT equivalent mass and the type of blast source are required as inputs. In addition, this function allows the user to obtain the pressure-time histories applied at each point. To check that the numerical models were subjected to a pressure similar to that of the field tests, pressure-time histories were obtained in all cases at the same position as the pressure gauges used in the experiment. Figure 16 shows an example of

the comparison between the numerical and experimental pressure signal for pressure gauge P1 in test E1. Similar agreement was obtained for the other tests (see Figure 11).

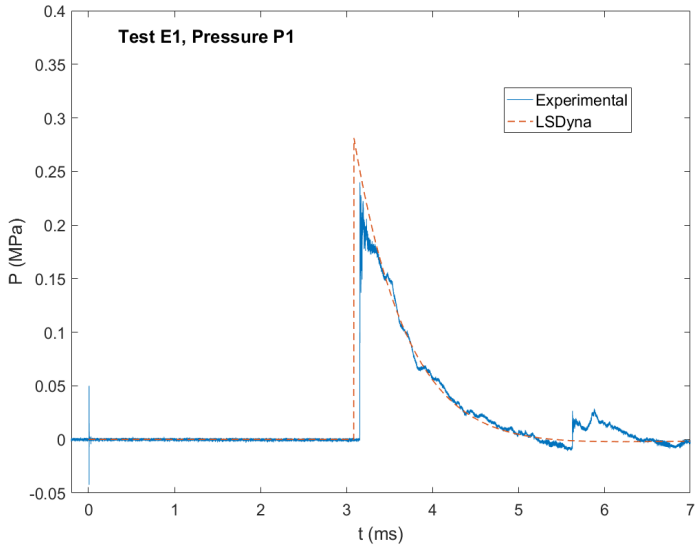

Figure 16 Pressure-time history of field test and numerical model.

Figure 17 shows the maximum displacements obtained in the simulation for the three different explosive charges used. It can be observed that the movement starts a few milliseconds after the start of the simulation. This time would correspond to the arrival time of the shockwave to the structure, which are 3.25 ms for test E1, 2.59 ms for tests E2/E3 and 2.14 ms for test E4. These times of arrival are very similar to those obtained in the experimental test shown in Table 3. In addition, the eigen-period for the first vibration mode can be also obtained, being consistently around 0.018 s.

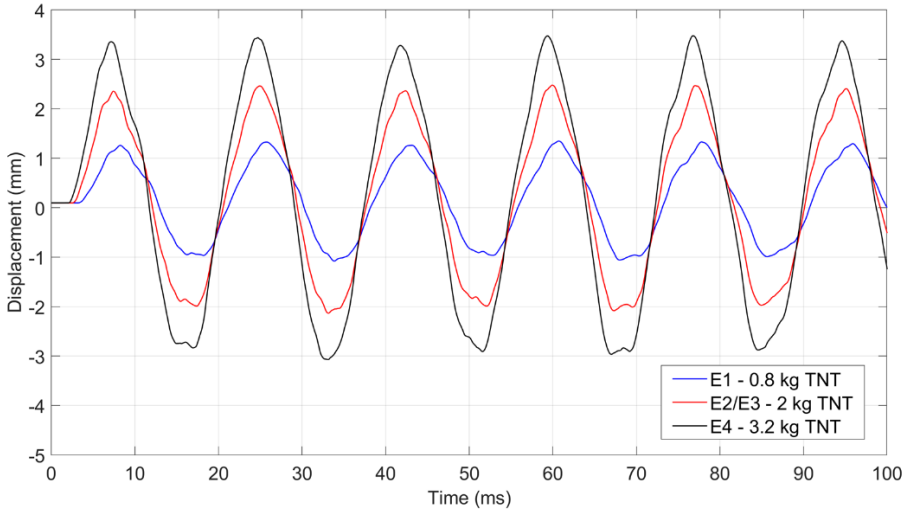

Figure 17 Result of maximum displacement.

5 Discussion

To determine the accuracy of the results obtained from the numerical simulation and the analytical model, these are compared with the results measured with the high-frequency laser used in the tests. As shown in Table 6, the values of maximum displacements calculated by numerical modelling and the SDOF dynamic calculations approximate quite well the values obtained experimentally. Looking at the different tests individually, it can be seen that, in the case of tests E1 and E4, the displacement of the SDOF model are closer to the experimental test than that obtained by the FEM. However, the displacement signal recorded in test E1 was the most unclear of all. For the other two tests (E2, E3) displacements obtained by the FEM are closer to the experimental values, being practically the same in the case of test E3. Regarding the fundamental eigen-period, the values provided by both models (analytical and numerical) are also in good agreement with the experimental values, although in this case, numerical simulation is again more accurate, as expected. With respect to the arrival times obtained by the FEM, they are, in all cases, within the range of the values obtained in the experimental tests. The largest

errors seem to be in the maximum measured pressures. This is not surprising as it is a point value and therefore liable to larger variability, which can be affected by the imperfect geometry of the explosive load (which is not a perfect sphere). On the other hand, the measured impulse, which is more stable as it is obtain by integrating the pressures and more significant because it has a greater influence in the response of the structure, seems to be better aligned with the initial estimates. It is surprising that while the measured pressures and the measured impulse in test E3 are larger than in test E2, the response of the structure is smaller in E3 than E2. This again must be attributed to the local character of the pressure measurements and the imperfection in the geometry of the explosive load (note that in E1, P2 and P3, which are theoretically symmetrical do not measure the same values – see Table 3). The deflections are the most global measurement of the structural response, and the one that best reflects the global effect of the action.

Table 6 Comparison of results between experimental test, numerical model, and analytical model.

		E1		E2		E3		E4	
Magnitude	Source	Meas. or Est.	Model/Exp	Meas. or Est.	Model/Exp	Meas. or Est.	Model/Exp	Meas. or Est.	Model/Exp
Displacement (mm)	Laser	0.95	-	2.7	-	2.53	-	3.2	-
	FEM	1.36	1.43	2.5	0.93	2.5	0.99	3.48	1.09
	SDOF	1.07	1.13	2.13	0.79	2.13	0.84	3.11	0.97
Eigen-period (s)	Laser	0.019	-	0.019	-	0.019	-	0.021	-
	FEM	0.018	0.95	0.018	0.95	0.018	0.95	0.018	0.86
	SDOF	0.016	0.84	0.016	0.84	0.016	0.84	0.016	0.76
Arrival time (s)	Laser	3.2 – 3.5	-	2.3 – 2.6	-	2.3 – 2.6	-	2.0 – 2.2	-
	FEM	3.25	0.97	2.59	1.06	2.59	1.06	2.14	1.02
Reflected pressure (kPa)	Pressure sensors P1/P2	210.1	-	673	-	841.3	-	1393	-
	Dod	265	1.26	643	0.96	643	0.76	1137	0.82
Impulse (kN.ms)	Pressure sensors P1/P2	123.3	-	299.1	-	329.6	-	436	-
	Dod	152.3	1.24	345.1	1.15	345.1	1.05	439.1	1.01

As an example, Figure 18 shows the comparison between the signal recorded with the high-frequency laser in tests E2 and E3 (both carried out with 2 kg TNT equivalent) and the signal obtained by the numerical simulation and the simplified analysis. To represent the signal obtained by SDOF calculations, the eigen-period and maximum displacement have been used to create a sinusoidal curve.

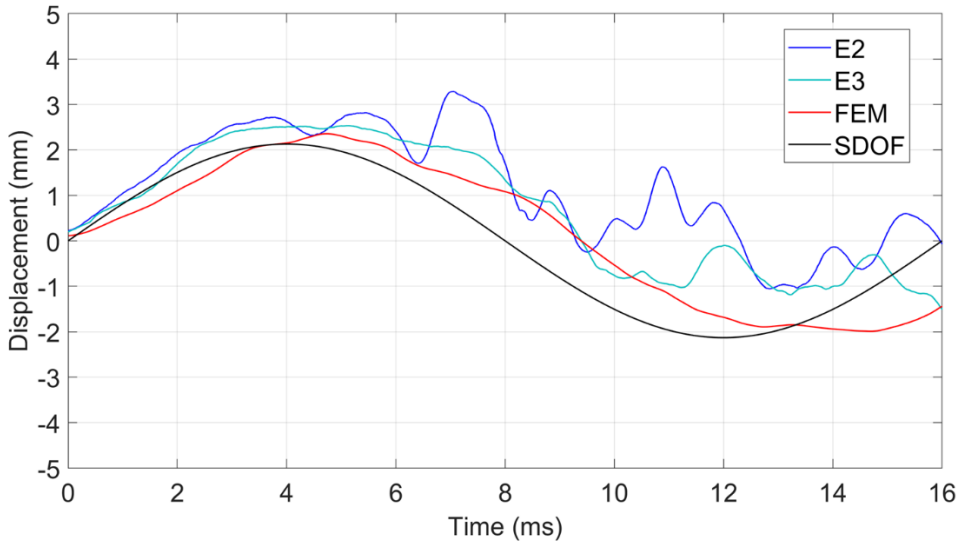

Figure 18 Result of maximum displacement with 2kg TNT equivalent: experimental values, numerical modelling, and theoretical dynamic calculations.

The SDOF analysis seems to provide a consistently stiffer response than the FEM and the actual specimen. This is due to the difference in the estimated period of the structure (0.016 s for the SDOF system, 0.018 s for the FEM and 0.019 s measured in the structure). For example, for T_E=0.016 s and t_{fr} = 0.77 ms (corresponding to E3 – see Table 1) the DLF is equal to 0.150, while this value would be 0.127 for a period of T_E=0.018 s. This difference (15% on the value of DLF) is more than enough to explain this result.

As shown in *Table 2*, the expected maximum stresses are very much within the elastic range (by a factor of close to 3). This is corroborated by the FEM analysis and the experimental results since the maximum displacement are within a similar range as those of the theoretical expectations.

6 Conclusions

A total of four experimental tests were carried out with the objective of evaluating the blast action by measuring the response of the structure. For this purpose, a steel structure was designed to withstand three different levels of blast load exhibiting an elastic response. These tests were then used to assess whether the response of the structure is consistent with the initial theoretical dynamic calculations and finite element numerical models using LS-DYNA. This evaluation has been made comparing the pressure-time curves and the displacements measured by a high-frequency laser scanner. After the evaluation, the following conclusions can be drawn:

1. Measurements obtained by the laser scanner are consistent along the different tests (i.e. displacements increase with the explosive charge).
2. SDOF simplified theoretical dynamic calculations estimate well both the eigen-period and maximum displacements, but numerical modelling shows a better approximation to experimental results, as expected since it accounts for the presence of the two adjacent beams. The main issue is that the SDOF is stiffer than the FEM and the physical model, leading to a higher value of the DLF.
3. The arrival time of the shockwave in the numerical model is in all cases within the range of values registered experimentally.
4. The test confirms that analyses carried out using measured or theoretical time-pressure curves provide a good approximation to the test results. These tests therefore constitute a validation for the usual simplified analysis methodologies.

As a lesson learned, the authors recommend shielding the laser from light. This could be done by using aluminum paper wrapped around a very flexible spring which should be in contact with the structure and the base of the laser.

Acknowledgements

This research was conducted under the ITSAFE project (Safe Transport Hubs against Heavy Explosions), funded by the Spanish Ministry for Economy and Competitiveness (IPT-2012-0845-370000). The project was led by Dragados and also integrated by FHECOR and Universidad Politécnica de Madrid (UPM). We would like to thank all the people who contributed to the design and execution of the tests. We also thank the staff in La Marañosa (ITM−INTA) for their help at the testing site.

References

[1] Institute for Economics and Peace, (2026), Global Terrorism Index 2026: Measuring the impact of terrorism, Sydney, Institute ofr Economics and Peace, http://visionofhumanity.org/resources.

[2] Biggs, J.M., (1964), Introduction to Structural Dynamics, McGraw-Hill College.

[3] El-Dakhakhni, W.W., Mekky, W.F., Changiz-Rezaei, S.H., (2009), Vulnerability Screening and Capacity Assessment of Reinforced Concrete Columns Subjected to Blast, Journal of Performance of Constructed Facilities 23(5): 353–65, https://doi.org/10.1061/(ASCE)CF.1943-5509.0000015.

[4] Gagnet, E.M., Hoemann, J.M., Davidson, J.S., (2017), Assessment of resistance definitions used for blast analysis of unreinforced masonry walls, International Journal of Protective Structures 8(1): 125–51, https://doi.org/10.1177/2041419617697518.

[5] Edri, I.E., Yankelevsky, D.Z., (2018), Analytical model for the dynamic response of blast-loaded arching masonry walls, Engineering Structures 176: 49–63, https://doi.org/10.1016/j.engstruct.2018.08.053.

[6] Hidallana-Gamage, H.D., Thambiratnam, D.P., Perera, N.J., (2014), Numerical modelling and analysis of the blast performance of laminated glass panels and the influence of material parameters, Engineering Failure Analysis 45: 65–84, https://doi.org/10.1016/j.engfailanal.2014.06.013.

[7] Remennikov, A.M., Rose, T.A., (2005), Modelling blast loads on buildings in complex city geometries, Computers & Structures 83(27): 2197–205, https://doi.org/10.1016/j.compstruc.2005.04.003.

[8] Zhao, C.F., Chen, J.Y., Wang, Y., Lu, S.J., (2012), Damage mechanism and response of reinforced concrete containment structure under internal blast loading, Theoretical and Applied Fracture Mechanics 61: 12–20, https://doi.org/10.1016/j.tafmec.2012.08.002.

[9] Jayasooriya, R., Thambiratnam, D.P., Perera, N.J., Kosse, V., (2011), Blast and residual capacity analysis of reinforced concrete framed buildings, Engineering Structures 33(12): 3483–95, https://doi.org/10.1016/j.engstruct.2011.07.011.

[10] Draganić, H., Gazić, G., Varevac, D., (2019), Experimental investigation of design and retrofit methods for blast load mitigation – A state-of-the-art review,

Engineering Structures 190: 189–209, https://doi.org/10.1016/j.engstruct.2019.03.088.
[11] Goswami, A., Adhikary, S.D., (2019), Retrofitting materials for enhanced blast performance of Structures: Recent advancement and challenges ahead, Construction and Building Materials 204: 224–43, https://doi.org/10.1016/j.conbuildmat.2019.01.188.
[12] Guo, Z., Xu, Z., Chen, C., Zhang, B., Lehman, D.E., Cao, S., (2017), Behavior of GFRP retrofitted reinforced concrete slabs subjected to conventional explosive blast, Materials and Structures 50(6): 236, https://doi.org/10.1617/s11527-017-1107-6.
[13] Xiao, W., Andrae, M., Steyerer, M., Gebbeken, N., (2021), Investigations of blast loads on a two-storeyed building with a gable roof: Full-scale experiments and numerical study, Journal of Building Engineering 43: 103111, https://doi.org/10.1016/j.jobe.2021.103111.
[14] Chiquito, M., López, L.M., Castedo, R., Santos, A.P., Pérez-Caldentey, A., (2023), Full-Scale Field Tests on Concrete Slabs Subjected to Close-In Blast Loads, Buildings 13(8): 2068, https://doi.org/10.3390/buildings13082068.
[15] Pérez Caldentey, A., Ferrero, I., Madrid, M., Corres, H., (2014), Simplified analysis of blast loading of limited intensity. A practical approximation for practical design, Madrid, ache.
[16] Department of Defense, (2008), UFC 3-340-02, Structures To Resist the Effects of Accidental Explosions, Washington D.C.
[17] Comité Européen de Normalisation (CEN), (2006), Eurocode 3 - Design of steel structures - Part 1-5: Plated structural elements., Brussels, CEN.
[18] Kingery, C.N., Bulmarsh, G., (1984), Air blast parameters from TNT spherical air burst and hemispherical burst., Aberdeen Proving Ground, MD, U.S. Army Ballistic Research Laboratory.